









RESEARCH ARTICLE

Estimating stratospheric polar vortex strength using ambient ocean-generated infrasound and stochastics-based machine learning

Ekaterina Vorobeva^{1,2}  | Mari Dahl Eggen^{2,3}  | Alise Danielle Midtjord^{3,4}  |
Fred Espen Benth³  | Patrick Hupe⁵  | Quentin Brissaud²  | Yvan Orsolini^{1,6}  |
Sven Peter Näsholm^{2,7} 

¹Department of Physics, Norwegian University of Science and Technology, Trondheim, Norway

²NORSAR, Kjeller, Norway

³Department of Mathematics, University of Oslo, Oslo, Norway

⁴Intellectual Labs AS, Oslo, Norway

⁵BGR, B4.3, Hanover, Germany

⁶Norwegian Institute for Air Research, Kjeller, Norway

⁷Department of Informatics, University of Oslo, Oslo, Norway

Correspondence

Sven Peter Näsholm, Department of Informatics, University of Oslo, Oslo, Norway and NORSAR, Kjeller, Norway.
Email: svenpn@ifi.uio.no

Funding information

NORSAR; Norges Forskningsråd, Grant/Award Numbers: Grant/Award Numbers: 223252/F50, 274377

Abstract

There are sparse opportunities for direct measurement of upper stratospheric winds, yet improving their representation in subseasonal-to-seasonal prediction models can have significant benefits. There is solid evidence from previous research that global atmospheric infrasound waves are sensitive to stratospheric dynamics. However, there is a lack of results providing a direct mapping between infrasound recordings and polar-cap upper stratospheric winds. The global International Monitoring System (IMS), which monitors compliance with the Comprehensive Nuclear-Test-Ban Treaty, includes ground-based stations that can be used to characterize the infrasound soundscape continuously. In this study, multi-station IMS infrasound data were utilized along with a machine-learning supported stochastic model, Delay-SDE-net, to demonstrate how a near-real-time estimate of the polar-cap averaged zonal wind at 1-hPa pressure level can be found from infrasound data. The infrasound was filtered to a temporal low-frequency regime dominated by microbaroms, which are ambient-noise infrasonic waves continuously radiated into the atmosphere from nonlinear interaction between counter-propagating ocean surface waves. Delay-SDE-net was trained on 5 years (2014–2018) of infrasound data from three stations and the ERA5 reanalysis 1-hPa polar-cap averaged zonal wind. Using infrasound in 2019–2020 for validation, we demonstrate a prediction of the polar-cap averaged zonal wind, with an error standard deviation of around $12 \text{ m}\cdot\text{s}^{-1}$ compared with ERA5. These findings highlight the potential of using infrasound data for near-real-time measurements of upper stratospheric dynamics. A long-term goal is to improve high-top atmospheric model accuracy, which can have significant implications for weather and climate prediction.

KEYWORDS

ambient noise, machine learning, microbarom infrasound, stratospheric polar vortex diagnostics

Ekaterina Vorobeva and Mari Dahl Eggen contributed equally to this study.

This is an open access article under the terms of the [Creative Commons Attribution](https://creativecommons.org/licenses/by/4.0/) License, which permits use, distribution and reproduction in any medium, provided the original work is properly cited.

© 2024 The Authors. *Quarterly Journal of the Royal Meteorological Society* published by John Wiley & Sons Ltd on behalf of the Royal Meteorological Society.

1 | INTRODUCTION

The zonally averaged stratospheric circulation at high northern latitudes is characterized by pronounced jets that flow eastward in the cold season and westward in the warm season. The prevailing wintertime eastward stratospheric flow is regularly disturbed by planetary waves that propagate from below, occasionally leading to either a temporary weakening or a reversal to a summer-like westward mean flow, associated with phenomena called minor and major stratospheric sudden warmings (SSWs). SSW events and their onsets can be defined in various ways, with most definitions involving stratospheric zonal winds and temperatures at the 10-hPa pressure level (see, e.g., Butler *et al.*, 2015; Baldwin *et al.*, 2021, for reviews). Although the 10-hPa pressure level is more commonly involved in the SSW definitions, these dramatic disruptions of atmospheric circulation affect the entire atmospheric column, from the troposphere to the thermosphere, across a broad range of latitudes (Limpasuvan *et al.*, 2016; Orsolini *et al.*, 2022; Pedatella, 2023; Pedatella *et al.*, 2018). SSW events, that can last for several days to week (Orsolini *et al.*, 2018), have an impact on tropospheric weather and climate patterns, such as cold-air outbreaks over North America and Eurasia (Kolstad *et al.*, 2010), southward jet-stream displacements over the Euro-Atlantic sector, and the negative phase of the North Atlantic Oscillation (Butler *et al.*, 2017). An episodic strengthening of the stratospheric eastward jet can also occur with a mirrored signature in the troposphere (Baldwin & Dunkerton, 2001; Limpasuvan *et al.*, 2005; Orsolini *et al.*, 2018).

Enhancing the representation of stratospheric dynamics in models can improve long-range weather prediction, particularly during winter (e.g., Domeisen *et al.*, 2020a, 2020b; Scaife *et al.*, 2022, and the references therein). Considerable efforts have been made at operational meteorological centers to improve the prediction of the stratospheric circulation (Karpechko, 2018; Scaife *et al.*, 2016) and of SSWs in particular. State-of-the-art seasonal or subseasonal-to-seasonal (S2S) dynamical ensemble prediction systems are coupled ocean-atmosphere models that extend into the stratosphere or above. For example, the most recent operational Seasonal Prediction System (SEAS5) at the European Centre for Medium-Range Weather Forecasts (ECMWF) extends up to 0.01 hPa, or about 90 km altitude (Johnson *et al.*, 2019). Ensembles of forecasts are then produced, initialized from analyses generated by data assimilation of a large amount of atmospheric, surface, and oceanic multi-platform observations (e.g., satellites, balloons, weather stations, aircraft, ships, buoys, etc.).

Low-frequency infrasound waves resulting from interactions between ocean surface waves moving in

opposite directions, known as microbaroms (Benioff & Gutenberg, 1939), can travel for extended distances. Microbaroms are quasi-continuous in time and are globally observed at infrasound stations of the International Monitoring System (IMS; see, e.g., Marty, 2019) in both hemispheres (De Carlo *et al.*, 2021; Hupe *et al.*, 2022). This is attributed to low attenuation and efficient stratospheric ducting, occurring between the ground and the stratopause at ~ 50 km altitude, corresponding to a pressure level of around 1 hPa (Drob *et al.*, 2003; Hupe *et al.*, 2019; Le Pichon *et al.*, 2006). The propagation of infrasound waves in the atmosphere is governed by wind and temperature fields (Diamond, 1963), and it has previously been shown in the literature that infrasound signals can serve as a tool for probing atmospheric dynamics (Le Pichon *et al.*, 2010, 2019, and the references therein). Pioneering work in the domain of microbarom-based atmospheric observation was performed by Donn, Rind and co-authors in several studies: for example, Donn and Rind (1971) and Rind and Donn (1975). Later, the potential to use such data to observe stratospheric wind variability was further demonstrated: for example, by Le Pichon *et al.* (2006), who analyzed 5 years of microbarom detections.

Machine learning has brought about a revolutionary change in data-driven research and is receiving considerable attention in the field of numerical weather prediction (e.g., Charlton-Perez *et al.*, 2023, and the references therein). Deep-learning-based approaches not only have the potential to replace traditional end-to-end data assimilation, but may also facilitate bias correction and calculation speed-up (Cheng *et al.*, 2023; Schultz *et al.*, 2021). Recent experiments involving the use of ERA5 reanalysis in the training have shown potential for machine learning in operational forecasting (Ben-Bouallegue *et al.*, 2023). Lam *et al.* (2023) demonstrated that a machine-learning model trained on ERA5 data outperformed the High RESolution forecast (HRES) system of ECMWF at up to 10 days lead time. S2S forecasting can also benefit from hybrid machine-learning and mixed approaches (Cohen *et al.*, 2019).

Building a physics-based model that relates infrasound data directly to atmospheric properties in near-real time is a challenging task and an active area of research. This would require fast and accurate modeling tools that are not yet available to the community. Alternatively, deep-learning approaches have recently gained interest by leveraging the sheer amount of continuous weather and infrasound data streams to perform various tasks, including automatic classification of coherent arrivals (Albert & Linville, 2020; Bishop *et al.*, 2022; Brissaud & Astafyeva, 2022; Liszka, 2008; Witsil *et al.*, 2022) or transmission loss modeling (Brissaud *et al.*, 2023). In particular,

Albert (2022) built a recurrent neural network based on Long–Short Term Memory (LSTM) units to forecast temperature and wind profiles 12 h in advance up to 30 km using all available radiosonde observations 12 and 24 h before the current time. The network prediction was then evaluated against ERA5 reanalyses. This work also demonstrated the benefit of better constraints on infrasound propagation paths. Further developments based on this model may involve uncertainty quantification and exploring its limits in terms of overfitting and generalization.

In the current study, a first attempt is made to provide a robust stratospheric polar vortex diagnostic using high-latitude infrasound data. These data are used to train a stochastic-based machine-learning model called Delay-SDE-net (Eggen & Midtjord, 2023). This is a novel neural network model using a stochastic differential equation (SDE) in a time-series modeling framework. SDEs are differential equations to which a random function is added for the purpose of quantifying uncertainty: see, for example, Øksendal (2003). A recently developed strategy for time-series modeling within the field of machine learning is to represent the derivatives in deterministic differential equations as neural networks (Chen *et al.*, 2018), providing an example of physics-informed neural network models (Raissi *et al.*, 2019). A particular development of such physics-informed neural networks using a simple SDE (in place of deterministic differential equations) as a modeling framework is called SDE-net (Kong *et al.*, 2020). Further innovations have emerged from SDE-net: see, for example, Wang *et al.* (2021) and Hayashi and Nakagawa (2022). Delay-SDE-net is an example of such innovation, using a more complex SDE as the modeling framework, where past states of a system are also taken into account. This makes Delay-SDE-net more flexible, as it holds inherent memory. This trait is particularly beneficial in the prediction of weather variables.

The analysis carried out in this study spans the 7 years 2014–2020. Delay-SDE-net is trained to map microbarom observations at the three northernmost IMS infrasound stations and day of year (DOY) to the ERA5 zonal-mean zonal wind at 1 hPa averaged between 60° and 90° latitude (hereafter denoted as the polar-cap averaged zonal wind). We focus on this pressure level, because stratospherically ducted infrasound is typically the most sensitive to winds in the upper stratosphere, where sound waves refract back towards the ground, as shown in, for example, Drob *et al.* (2003), Le Pichon *et al.* (2006), and Hupe *et al.* (2019). Using years 2019 and 2020 as validation, we show that there is good agreement between ERA5 and the wind predicted by the infrasound-based machine-learning model. The dissimilarity between these datasets is estimated in terms of root-mean-square error (RMSE) and does not exceed 12 m·s⁻¹ for both validation years. The results

obtained reveal a possibility of using quasi-continuous microbarom observations for the near-real-time measurement of the zonally averaged polar stratospheric circulation. The purpose of this study is not to compete with existing comprehensive, ocean–atmosphere coupled model forecasts, but rather to demonstrate that infrasound observations can be used as an additional source of information to existing atmospheric models.

This article is organized as follows. The atmospheric and infrasound datasets are introduced and discussed in Sections 2.1 and 2.2. The stochastic-based machine learning approach is presented in Section 2.3. The results are collected and discussed in Section 3 and the study is concluded in Section 4.

2 | DATA AND METHODS

2.1 | ERA5 atmospheric reanalysis product dataset

As data assimilation schemes, computational performance, and forecast models evolve, the performance of atmospheric reanalyses improves. Today, the fifth generation of the ECMWF's atmospheric reanalysis, ERA5, has replaced the earlier ERA-Interim reanalysis (Dee *et al.*, 2011). ERA5 provides global hourly estimates of atmospheric, ocean-wave, and land-surface quantities with higher resolution compared with the previous ECMWF reanalysis products (Hersbach *et al.*, 2020). The atmospheric product has an approximate horizontal resolution of 0.28° × 0.28° and covers 1000–0.01 hPa or 0–90 km altitude (137 model levels). The ERA5 data are currently available from 1959 and have a latency of five days (Bell *et al.*, 2021), and their uncertainty is estimated from the 10-member ensemble with three-hourly temporal and 0.56° × 0.56° horizontal resolution. For an overview of the ERA5 strengths and biases and a comparison with other reanalyses, we refer the reader to Hersbach *et al.* (2020) and Bell *et al.* (2021).

In this study, the ERA5 zonal wind, U , at 1-hPa pressure level (~50 km altitude) is extracted from the ECMWF archive (see the Data Availability statement at the end of the article) for the years 2014–2020. The polar-cap averaged zonal wind, defined here as the zonal-mean zonal wind, cosine of latitude weighted and averaged between 60°–90° latitudes, $\bar{U}_{1\text{hPa}}$, is calculated for every day of the year based on the ensemble mean. For the leap years, February 29 is removed from consideration. The ensemble uncertainty (spread) is estimated on the basis of the standard deviation with respect to the mean. The ensemble mean and spread of $\bar{U}_{1\text{hPa}}$ for the 7 years considered are presented in Figure 1. In addition, we calculate a seasonal

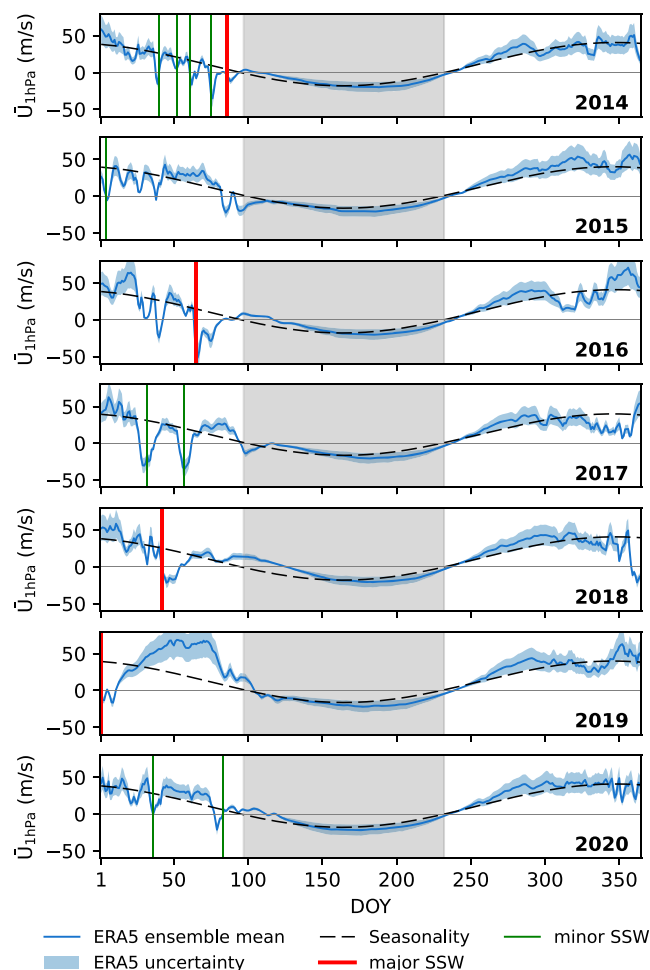


FIGURE 1 Polar-cap averaged zonal wind at 1 hPa for 2014–2020. ERA5 ensemble mean and spread are shown as a blue solid line and a blue shade, respectively. The Fourier-series-based seasonal cycle is plotted as a black dashed line. SSW events are indicated with vertical solid lines (major SSW, red; minor SSW, green). A gray shade highlights the warm season when the seasonal cycle has negative values. [Colour figure can be viewed at [wileyonlinelibrary.com](https://onlinelibrary.com)]

cycle by fitting the following Fourier series to the wind data:

$$y(t) = a_0 + \sum_{i=1}^2 a_i \cos(\omega_i t) + b_i \sin(\omega_i t), \quad (1)$$

where $\omega_i = i\pi/365 \text{ day}^{-1}$. The Fourier-series-based seasonal cycle is plotted in Figure 1 as a black dashed line.

Two features typical of the stratospheric circumpolar circulation can be seen from these plots. First, positive $\bar{U}_{1 \text{ hPa}}$ values (eastward jet) prevail in the cold season and negative values (westward jet) in the warm season. The warm season is estimated as days of the year 97–232 (gray shade in Figure 1) based on days when the $\bar{U}_{1 \text{ hPa}}$ seasonal cycle (found from a Fourier series fit to all years considered) changes sign. Second, the ERA5 uncertainty

is larger in winter due to the high temporal variability of the stratospheric jet in the Northern Hemisphere (Waugh *et al.*, 2017). Moreover, the strong deviations of the polar-cap averaged zonal wind from its seasonal average observed in Figure 1 are associated with SSW events, as indicated by vertical lines.

SSWs are typically associated with a sudden temperature increase at high latitudes and either zonal-mean flow weakening or reversal at mid and high latitudes. A recent review on SSWs can be found in Baldwin *et al.* (2021). During 2014–2020, four major (reversal of the zonal-mean flow at 10 hPa) and nine minor (weakening of the zonal-mean flow at 10 hPa) occurred. The major events occurred on March 27, 2014 (de Jesus *et al.*, 2017), March 5–6, 2016 (Manney & Lawrence, 2016), February 11, 2018 (Pérot & Orsolini, 2021; Rao *et al.*, 2018), and January 1, 2019 (Pérot & Orsolini, 2021; Rao *et al.*, 2019). The onsets of the minor events are estimated as February 9 and 19, 2014, March 1 and 16, 2014 (de Jesus *et al.*, 2017), January 4, 2015 (Manney *et al.*, 2015), February 1 and 26, 2017 (Eswaraiah *et al.*, 2019, 2020), and February 5 and March 23, 2020 (Yin *et al.*, 2023). The minor SSWs are presented in Figure 1 as vertical green lines, and major events as red vertical lines. In most cases, we see that the $\bar{U}_{1 \text{ hPa}}$ values change sign from positive to negative shortly before the onset estimated at the standard 10-hPa pressure level. This effect, with a change in zonal wind initiated in the upper stratosphere (1 hPa) descending to the mid-stratosphere (10 hPa), was reported previously (e.g., Limpasuvan *et al.*, 2016; Shepherd *et al.*, 2014; Vignon & Mitchell, 2015; Zülicke & Becker, 2013, and references therein). A detailed analysis of such extreme events is not the focus of this study; however, we would like to highlight the potential of using \bar{U} at 1 hPa for SSW identification in further studies.

2.2 | Infrasound dataset

Microbaroms are the dominating signals in infrasound ambient noise and span the frequency range of 0.1–0.6 Hz, with a peak frequency of ~ 0.2 Hz. These waves are detected globally throughout the year, as shown by De Carlo *et al.* (2021) based on observations at 45 IMS infrasound stations in both hemispheres. Under wind conditions that favor acoustic waveguides, microbaroms propagate over large distances in the atmosphere (e.g., Donn & Rind, 1971; Garcés *et al.*, 2004; Le Pichon *et al.*, 2006). The dominating frequency of microbaroms depends on the size of the water basins, with higher frequencies typical for spatially limited water areas and coastlines (e.g., Hupe *et al.*, 2019). As the main focus of this study is on characterizing the stratospheric circulation on a large scale, microbaroms generated by large water basins are of the greatest interest.

To this end, a low-frequency (0.15–0.35 Hz) microbarom dataset from Hupe *et al.* (2021, 2022) is used. The dataset is generated from IMS infrasound station data using the Progressive Multi-Channel Correlation (PMCC) array signal-processing approach (Cansi, 1995; Cansi & Le Pichon, 2008; Kristoffersen *et al.*, 2022) and output parameters include wavefront characteristics as a function of time under the assumption of a far-field plane-wave model. Among other output parameters, the processing of Hupe *et al.* (2022) provides a quality parameter, Q , for the data at each time sample. This parameter is based on the number of available sensors, the number of sensors contributing to a PMCC detection, and correlation between sensors, as well as the Fisher ratio (see eq. (1) in Hupe *et al.*, 2022). The Q parameter is distributed between 0 and 1, and we set a threshold of $Q > 0.4$ to perform our further analysis using only the high-quality data. To focus on stratospherically ducted microbarom arrivals, we also excluded some data points based on the apparent velocity, V_{app} , which is the plane-wave horizontal velocity as it propagates along the array. Previous works have demonstrated that, for microbaroms propagating in stratospheric ducts, V_{app} is typically in the 340–380 m·s⁻¹ range (see, e.g., Vorobevo *et al.*, 2021, and the references therein). We removed all data points with $V_{\text{app}} > 380$ m·s⁻¹. Microbarom detections from all back azimuths were used.

Microbarom data from the three northernmost IMS infrasound arrays (IS18, IS37, and IS53) located within the polar cap are utilized in this study. Table 1 presents information about these arrays, such as location, number of sensors, and aperture. Note that the IS37 array was certified 10 years later than IS18 and IS53. Given the time span of processed microbarom infrasound data from these stations available in Hupe *et al.* (2021), our study considers 7 years of data between 2014 and 2020. Figure 2 shows the location of the three arrays on the map, together with their geometrical configurations and the directional distributions of microbarom detections for the cold and warm seasons. For every day of the year, we extract information about the strongest microbarom source, namely, the maximum microbarom amplitude and the corresponding back azimuth. For times when there were no data available (4.8%, 14.8%, 13.5% for IS18, IS37, and IS53, respectively), the amplitude and back-azimuth values are replaced with the mean values for that specific day calculated based

on the 7-year dataset. Typical reasons for missing data are equipment failure, array maintenance, or weather conditions (Marty, 2019).

Figure 3 displays the daily variations in microbarom amplitude and back azimuth over the course of 7 years. The microbarom amplitudes for all three stations have a pronounced seasonal pattern, with the highest amplitudes being recorded in winter. This pattern is similar to the seasonal variations of $\bar{U}_{1\text{hPa}}$ also plotted in Figure 3. This can be explained by the enhanced microbarom source activity in winter coinciding with the eastward stratospheric wind, beneficial for ducting infrasound waves over long distances (De Carlo *et al.*, 2021; Landès *et al.*, 2012; Le Pichon *et al.*, 2006). The same effect occurs in the Southern Hemisphere during the austral winter (Le Pichon *et al.*, 2006).

From the directional distributions of microbarom signals presented in Figures 2 and 3, a certain seasonal pattern can also be seen for each of the stations. For IS37, the signals arriving from the North Atlantic (255°–260° back azimuth) dominate throughout the year, with additional detections from the Barents Sea (10°–15°) during the warm season. Microbaroms generated in the North Atlantic are also regularly observed at IS18, with competing signals arriving from around 270°–300° in winter. In the warm season, arrivals from two source regions in the North Atlantic are detected with back-azimuth values of 125°–130° and 145°–150°. At IS53, southwest arrivals from the Pacific Ocean dominate in winter, whereas during the warm season additional sources are detected from the south and northeast.

2.3 | Stochastic modeling and the Delay-SDE-net

Classically, ordinary and partial differential equations are used to represent physical systems in time and space. These are deterministic relations derived on the basis of physical laws and are restricted to systems with strict constraints. It is not possible to describe most dynamical systems exactly, either because they are too complex or because of natural randomness. In many cases, it is sufficient to model such systems stochastically, which means that the evolution of the system is associated with

TABLE 1 Details of the infrasound arrays used in the study.

Array	Location (°N, °E)	Elevation (m)	N_{sensors}	Aperture (km)	Certified in
IS18	(77.48, -69.29)	69	8	1.16	2003
IS37	(69.07, 18.61)	74	10	1.95	2013
IS53	(64.88, -147.86)	200	8	1.97	2003

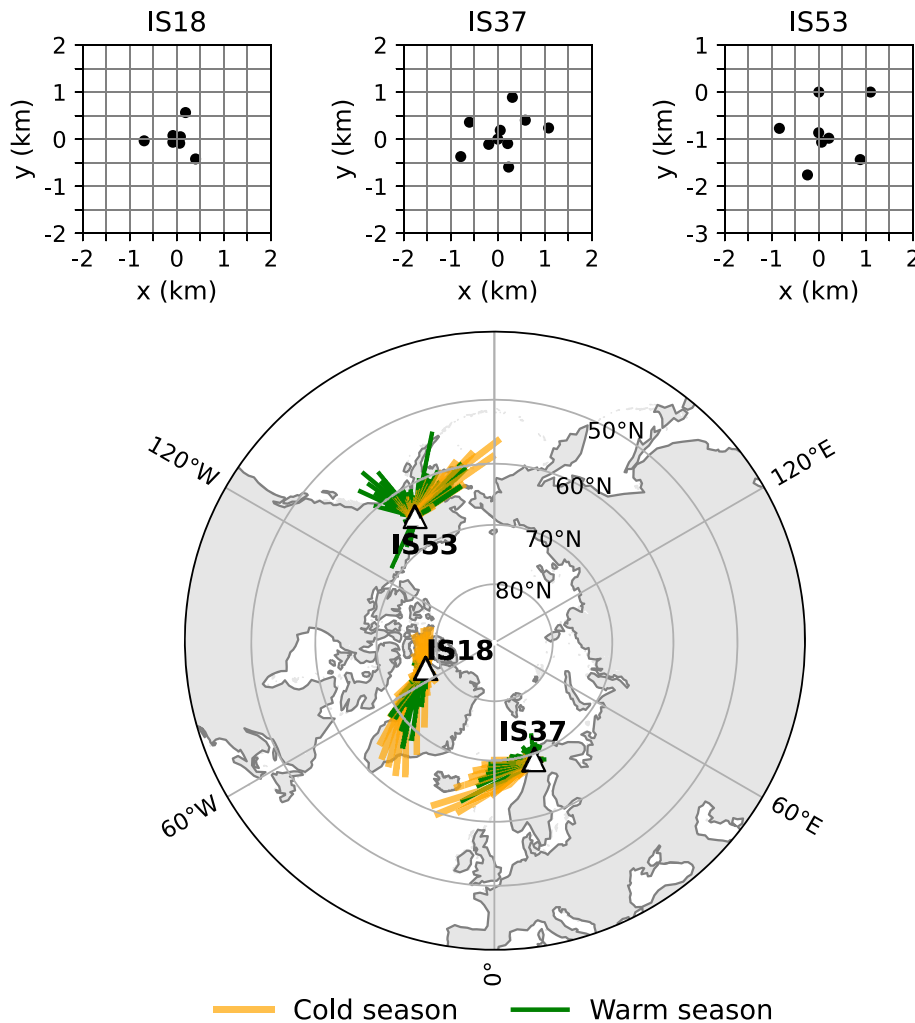


FIGURE 2 The IMS infrasound arrays used in this study and their geometrical configurations. The directional distributions of microbarom detections are plotted for the cold (orange) and warm (green) seasons. [Colour figure can be viewed at [wileyonlinelibrary.com](https://onlinelibrary.wiley.com/doi/10.1002/qj.4731)]

a certain probability distribution. This is done by representing a dynamical system as accurately as possible using deterministic differential equations, where a stochastic term is added to represent uncertainty. Such modeling frameworks are called SDEs.

It is established in the literature that dynamical systems of weather variables are well represented by statistical linear autoregressive models (e.g., Benth *et al.*, 2008; Benth & Benth, 2010; Broszkiewicz-Suwaj & Wyłomańska, 2021; Campbell & Diebold, 2005; Eggen, 2022; Eggen *et al.*, 2022). Overviews and implementations of such models are provided in Brockwell and Davis (2016) and Gómez (2019). The continuous-time counterparts of such models are linear systems of SDEs (e.g., Brockwell, 2004, 2014; Marquardt & Stelzer, 2007). In the current work we consider a multivariate dynamical system consisting of polar-cap averaged zonal wind at 1 hPa, data-processing output variables retrieved from infrasound array recordings, and also DOY.

Results from our initial analysis of the datasets lead to the assumption that co-variations between stratospheric wind and infrasound variables are non-stationary and/or

nonlinear. Based on this, we chose a so-called stochastic delay differential equation (SDDE) as modeling framework. Note that the SDDE is a generalized version of the continuous-time linear autoregressive model (Basse-O'Connor *et al.*, 2020). The SDDE is a multivariate (possibly non-stationary and nonlinear) SDE explaining co-variation between variables of a dynamical system, as well as co-variation between time-lagged versions of these variables. This ability applies to both the deterministic and stochastic (uncertainty) parts of the model. When the SDDE is used as a modeling framework, due to its generality, a suitable model can be challenging to work out.

A novel methodology for elaborating such frameworks using neural networks is derived by Eggen and Midtjord (2023), where Delay-SDE-net is presented. The Delay-SDE-net model can be considered as a discrete-time SDDE where the model coefficients are independent neural networks. The model trained for this work makes a near-real-time prediction and is of the form

$$\hat{w}_t = f(t, \mathbf{x}_{t-p-1}, \dots, \mathbf{x}_t)\Delta t + g(t, \mathbf{x}_{t-p-1}, \dots, \mathbf{x}_t)\epsilon_t, \quad (2)$$

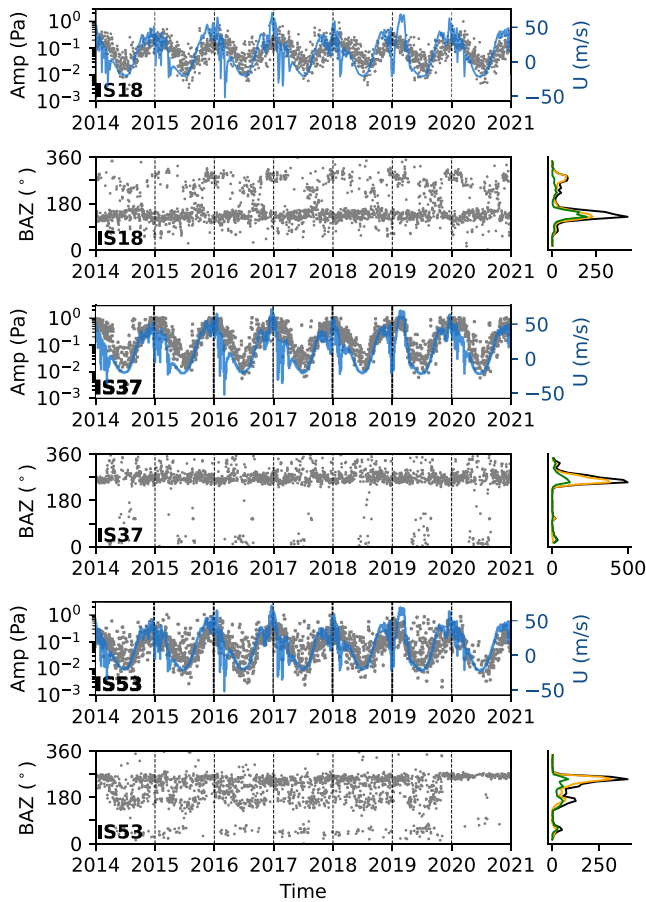


FIGURE 3 Amplitude and back azimuth of the strongest microbarom detection per day over the course of 7 years accompanied by ERA5 polar-cap averaged zonal wind at 1 hPa (blue). The infrasound station code is indicated in the plot. The right panels present the back-azimuth distributions calculated for 10° bins (black) as well as distributions for cold (orange) and warm (green) seasons. [Colour figure can be viewed at [wileyonlinelibrary.com](https://onlinelibrary.wiley.com/doi/10.1002/qj.4731)]

where $\Delta t = 1$ is the time-step size of one day, $p - 1$ is the number of time lags in the model, and $\epsilon_t \sim N(0, 1)$ is a standard normally distributed random variable. We use $p = 4$, following Eggen *et al.* (2022). Furthermore, $\mathbf{x}_s = [x_{s,1}, \dots, x_{s,9}]$, with $s = t - p - 1, \dots, t$, is a nine-dimensional vector of infrasound measurement values at time s , the functions f and g represent trained neural networks for the deterministic and stochastic parts of the model, respectively, and \hat{w}_t represents the corresponding estimated stratospheric wind, $\bar{U}_{1 \text{ hPa}}$. The input and output variables for this model are explained thoroughly in Sections 2.1 and 2.2. In particular, see Figures 1 and 3. The back-azimuth features are decomposed into their x - and y -directions, corresponding to the cosine and sine of the back-azimuth angle, respectively. This provides continuous ranges of back-azimuth features over all directions. As a result, the feature vector, \mathbf{x}_s , with infrasound measurements from three stations, holds nine variables,

consisting of three microbarom amplitudes and six values representing the cosine and sine of the back-azimuth values estimated at the stations.

As already implied, the deterministic part, f , of the trained Delay-SDE-net provides an expected value of $\bar{U}_{1 \text{ hPa}}$, and the stochastic part, g , is used to provide model uncertainty estimates. This is obtained by first training f by minimizing the prediction error of the training data compared with the ERA5 wind ($\hat{w}_t - w_t$). This procedure is followed by a training of g in two steps to capture both aleatoric and epistemic uncertainty (Der Kiureghian & Ditlevsen, 2009). The aleatoric uncertainty comes from the natural randomness inherent in the task and it captures the residuals from the deterministic net

$$\hat{w}_t = f(t, \mathbf{x}_{t-p-1}, \dots, \mathbf{x}_t) \Delta t. \quad (3)$$

The epistemic part can be considered as the uncertainty due to lack of knowledge within the model and provides a higher uncertainty estimate when the model sees unusual states or unusual combinations of states. For the stratospheric polar vortex, SSW events with strong deviations from the seasonal average can be considered unusual features. We therefore suggest that properties of the epistemic part could make a useful tool for assessment of SSW events and other stratospheric vortex anomalies.

We train Delay-SDE-net on 5 years (2014–2018) of infrasound data from three stations (Section 2.2), ERA5 ensemble-mean polar-cap averaged zonal wind $\bar{U}_{1 \text{ hPa}}$, and DOY. The validation is performed on years 2019 and 2020 based on the trained model, DOY, and infrasound observations. The trained stochastic part of Delay-SDE-net is used to provide prediction intervals (PIs) of $\bar{U}_{1 \text{ hPa}}$ predicted by Delay-SDE-net. The prediction confidence is given as 90% intervals. Since the expected value of wind is different for every day of the year, we consider the Delay-SDE-net wind estimates for each day of the year as independent populations. The training dataset consists of 5 years, meaning that we have sample size $n = 5$. The PIs are computed according to Devore *et al.* (2012) (their eq. (8.14)). See Figure 4 for the estimated PIs.

3 | RESULTS AND DISCUSSION

3.1 | Inferring the polar-cap averaged zonal wind based on microbarom infrasound recordings

The core results of this study are presented in Figure 4, which compares estimates of the polar-cap averaged zonal wind by the infrasound-based Delay-SDE-net and ERA5 (blue curve) for the validation years 2019

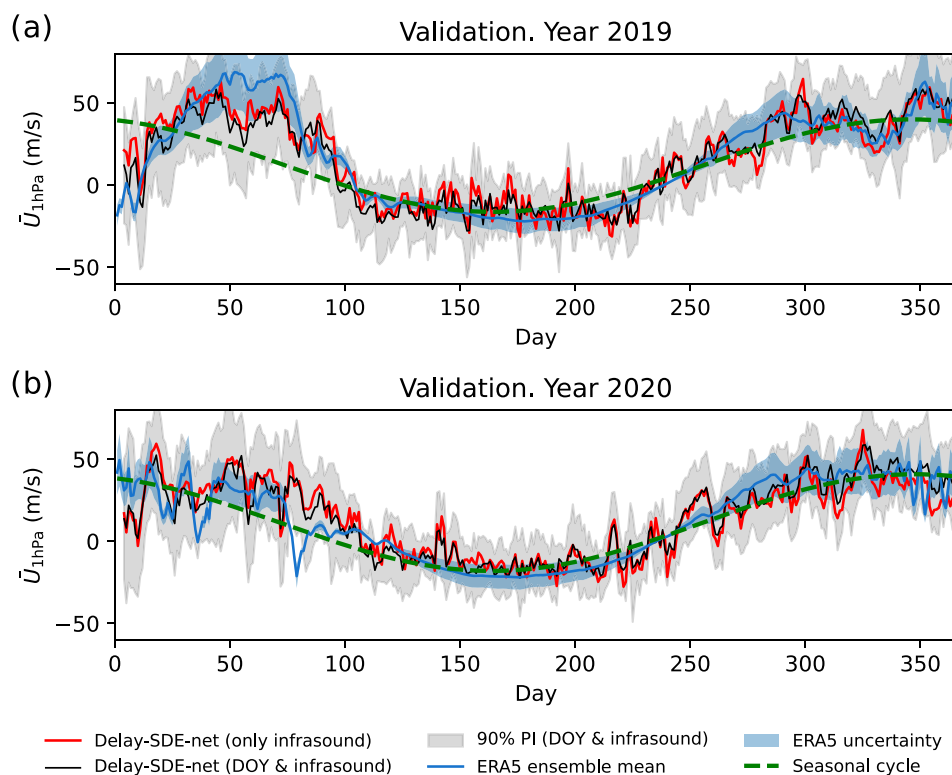


FIGURE 4 Comparison between the ERA5 and Delay-SDE-net estimates of the polar-cap averaged zonal wind at 1-hPa pressure level for (a) 2019 and (b) 2020. Blue: ERA5 ensemble mean; black: Delay-SDE-net estimate when trained on infrasound data and DOY; red: Delay-SDE-net estimate when trained on infrasound data only; green: Fourier-series-based seasonal cycle based on ERA5. The uncertainties are indicated with shaded areas: blue denoting ERA5 and gray denoting Delay-SDE-net trained on infrasound data and DOY. Note that the black and red curves correspond to Delay-SDE-net trained on microbarom amplitudes and back-azimuth data from all three infrasound stations (IS18, IS37, and IS53). [Colour figure can be viewed at wileyonlinelibrary.com]

and 2020. Note that data from these years were not seen in the Delay-SDE-net training. Two $\bar{U}_{1\text{hPa}}$ estimates by Delay-SDE-net are shown as black and red curves that represent instances where Delay-SDE-net was trained with and without incorporating information on the DOY, respectively. For comparison, we also display the Fourier-series-based seasonal cycle fit based on Equation (1) (green dashed curve). The $\bar{U}_{1\text{hPa}}$ estimates by ERA5 and Delay-SDE-net trained on infrasound and DOY are plotted together with their uncertainties. These are obtained from the ERA5 10-member ensemble spread (blue shade) and from the 90% PIs for Delay-SDE-net (gray shade).

Looking at the two realizations of Delay-SDE-net, we note that (1) the two approaches yield very similar results in both validation years, and (2) including the DOY in the training does not over-constrain the method to the seasonal cycle. This can be explained by the sensitivity of infrasound propagation to seasonal variations in stratospheric winds as discussed in Section 2.2. The RMSE over the years 2019 and 2020 between the ERA5 and Delay-SDE-net $\bar{U}_{1\text{hPa}}$ estimates is 11.3 and 11.5 $\text{m}\cdot\text{s}^{-1}$ respectively when the DOY is included, while the RMSE is 11.7 and 13.6 $\text{m}\cdot\text{s}^{-1}$ respectively when DOY is not included. As the Delay-SDE-net realization with the DOY included in the training provides slightly lower RMSE in this comparison, we will

include the DOY in simulations for the remainder of this study.

At the onset of 2019, a pronounced SSW is evident from the negative ERA5 $\bar{U}_{1\text{hPa}}$ values shown in Figure 4a. The Delay-SDE-net estimate of $\bar{U}_{1\text{hPa}}$ that includes DOY in the training captures this distinctive SSW feature effectively, aligning significantly more closely with the ERA5 ensemble mean than the Fourier-based seasonal cycle. However, it is noteworthy that, when Delay-SDE-net is trained exclusively on infrasound data, its $\bar{U}_{1\text{hPa}}$ estimate exhibits positive values up to DOY 11 and diverges significantly from the ERA5 estimate during this period. Despite this, a good agreement with the ERA5 ensemble mean is obtained throughout the year, with 96.9% and 98.1% of the ERA5 values falling within the Delay-SDE-net PIs when trained on both infrasound and DOY and exclusively on infrasound, respectively. Examining the $\bar{U}_{1\text{hPa}}$ amplitude during the recovery phase of the polar vortex, our analysis reveals the following findings. During days 45–80, the difference between ERA5 and Delay-SDE-net $\bar{U}_{1\text{hPa}}$ increases. The Delay-SDE-net estimate is approximately 20 $\text{m}\cdot\text{s}^{-1}$ smaller than the ERA5 ensemble mean. Notably, during days 51–57, the difference reaches up to 30–40 $\text{m}\cdot\text{s}^{-1}$. Subsequently, a much better agreement is observed for the remainder of the year, with the difference centered consistently around 5 $\text{m}\cdot\text{s}^{-1}$.

Figure 4b compares the ERA5 and Delay-SDE-net $\bar{U}_{1\text{hPa}}$ estimates for year 2020. From this display, it is clear that $\bar{U}_{1\text{hPa}}$ in 2020 is significantly closer to the seasonal cycle compared with 2019. As therefore expected, informing Delay-SDE-net with infrasound data in addition to the DOY turns out to provide less added value in 2020 compared with 2019, when there was more stratospheric variability. However, despite a generally good agreement in 2020, some discrepancies can be seen. For example, in the beginning of the year up to around day 15, both realizations of Delay-SDE-net estimate $\bar{U}_{1\text{hPa}}$ to be weaker compared with ERA5. In addition, the negative values of $\bar{U}_{1\text{hPa}}$ estimated by ERA5 around two minor SSWs (DOYs 35–37 and 78–82, respectively: Yin *et al.*, 2023) are not well predicted by Delay-SDE-net. Despite these discrepancies, a good agreement is obtained, with 96.6% and 95.3% of ERA5 values falling within the Delay-SDE-net PIs when trained on both infrasound and DOY and exclusively on infrasound, respectively.

3.2 | Sensitivity to the choice of infrasound stations and data

Figure 4 showed the results of Delay-SDE-net trained on microbarom amplitudes and back azimuths from all three infrasound stations (see Figure 2 and Table 1), but it is also important to assess the sensitivity of Delay-SDE-net to different combinations of infrasound stations and array-processing parameters. We therefore perform a sensitivity analysis for the validation years 2019 and 2020, where 21 scenarios are run for each year: seven different combinations of stations (single station, two stations, three stations) with three combinations of infrasound array data parameters (microbarom amplitude, back azimuth, both amplitude and back azimuth). Note that we use the Delay-SDE-net that includes DOY in the training, as stated in Section 3.1.

Figure 5 shows the sensitivity analysis results, with RMSEs plotted for different scenarios. For year 2019, with a lot of stratospheric wind variability and a major SSW, the difference between the ERA5 and Delay-SDE-net estimates decreases significantly when increasing the number of stations and array data-processing output parameters used. The lowest 2019 RMSE of $11.3\text{ m}\cdot\text{s}^{-1}$ is obtained when training Delay-SDE-net on all available infrasound data. In contrast, the RMSEs for year 2020, with relatively undisturbed stratospheric dynamics and no major SSW, remain consistent across the scenarios analyzed. This indicates that, for seasons like 2020, training Delay-SDE-net on observations from a single station yields a $\bar{U}_{1\text{hPa}}$ estimate of nearly the same quality as when utilizing infrasound

data from multiple stations. Nevertheless, a better estimate of $\bar{U}_{1\text{hPa}}$ is generally expected with observations from all three infrasound stations. The RMSE is within $10\text{--}14\text{ m}\cdot\text{s}^{-1}$ and reaches $11.5\text{ m}\cdot\text{s}^{-1}$ when training on the entire infrasound dataset.

We note that the combination of data from IS37 and IS18 gives a lower RMSE than the other station pair combinations, in particular for year 2019. A reason might be that these two stations are located at comparably close distances to the North Atlantic microbarom source hotspot (see Figure 2 and De Carlo *et al.*, 2020, 2021). They are thereby “illuminated” by this source from complementary back-azimuth directions, and the combined or complementary station detection/non-detection of microbaroms from this region might be particularly sensitive to the upper stratospheric wind morphology. For 2020, where there was less stratospheric polar vortex variability, there is limited added value in using data from multiple infrasound stations.

3.3 | Avenues for future work

To evaluate the performance of Delay-SDE-net comprehensively, it is proposed to blend the training and validation years, allowing for the generation of results encompassing all possible permutations across the 7 years of data. In addition, investigating the impact of incorporating the SSW events in the training dataset on their predictive performance during the validation stage presents an

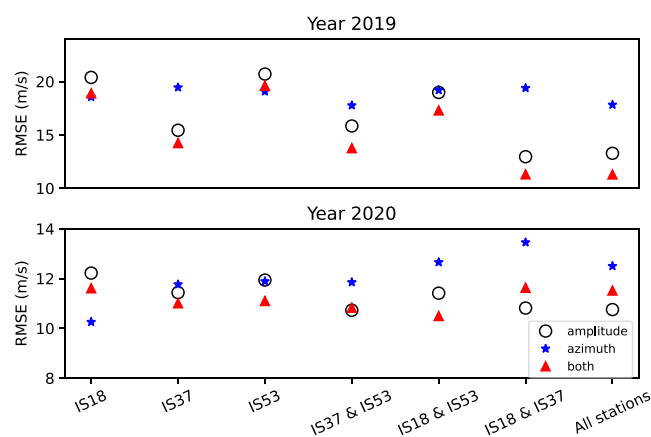


FIGURE 5 Sensitivity analysis of the infrasound and DOY based Delay-SDE-net to different combinations of training parameters for years 2019 (top panel) and 2020 (bottom panel). The RMSE between the ERA5 and Delay-SDE-net estimates of the polar-cap averaged zonal wind is plotted as a function of training parameters used. Note that the DOY is included in all these numerical experiments, and that panels have different limits for vertical axes. [Colour figure can be viewed at wileyonlinelibrary.com]

intriguing avenue for further exploration. Albeit irregular, major SSW events occur approximately every 2 years on average, and to obtain a dataset without them one would need to delve deeper into historical records and compile a training dataset from years without SSWs. Moreover, the epistemic uncertainty part of Delay-SDE-net, as explained in Section 2.3, has potential to, during inference, flag unusual events such as SSWs that are less common in the training data. Hence, a future study could exploit the epistemic uncertainty output of Delay-SDE-net to detect SSWs and other stratospheric anomaly events. Furthermore, a more detailed examination of different SSW types (vortex split or displacement) can be performed in order to define in which cases the infrasound-based machine-learning model performs better.

Microbaroms are generated by counter-propagating ocean waves, and their source field is dynamic in time and space. Therefore, an interesting further analysis could be to assess the benefits of also informing the machine-learning model about the microbarom source locations and strength as a function of time. Such microbarom generation and radiation models have been elaborated, for example, in De Carlo *et al.* (2020). Another possible direction of research could be to apply different infrasound array data-processing approaches. For example, the back azimuth and apparent velocity of several coherent infrasound arrivals can be obtained using the CLEAN algorithm (Högbom, 1974), as presented by den Ouden *et al.* (2020). Furthermore, a velocity spectral analysis (vespa) processing can be applied to microbarom observations in order to provide a directional distribution. Recently, Vorobeva *et al.* (2021) showed that vespa provides realistic estimates of microbarom soundscapes when compared with the state-of-the-art microbarom radiation and propagation model of De Carlo *et al.* (2020).

The Delay-SDE-net performance is fast (72 s for 2 years of data when DOY is included and 162 s when DOY is not included), and additional infrasound-based variables can be added straightforwardly. Another natural extension to the current work is to add data from more stations and to examine the prospects for a more fine-grained middle atmospheric probing in terms of both altitudes and geographical areas.

4 | CONCLUDING REMARKS

Microbarom observations at three polar IMS infrasound stations are proposed as an additional source of observational information on the upper stratospheric circulation, thereby addressing a wind observation gap at these altitudes. We developed a mapping that uses infrasound data from these stations and the DOY as input to provide an

estimate of the polar-cap averaged zonal wind at 1-hPa pressure level as output. The applied stochastic-based machine-learning model (Delay-SDE-net) is trained on a 5-year-long time series of processed microbarom infrasound data, the DOY, and the ERA5 ensemble mean polar-cap averaged zonal wind. In the inference stage, the model is informed about the infrasound data and the DOY. In addition, we showed that the mapping also works well without involving the DOY in training and inference.

On the basis of 2 years of validation, it is demonstrated that the Delay-SDE neural network informed by ground-based infrasound observations and DOY performs well in predicting the ERA5 polar-cap averaged zonal wind with an RMSE of around $12 \text{ m}\cdot\text{s}^{-1}$. Moreover, a series of additional numerical experiments were conducted to explore the sensitivity of the Delay-SDE-net output to the number of infrasound stations and the amount of array data-processing output parameters. For year 2019 with a major SSW, the RMSE between the ERA5 ensemble mean and the infrasound-based polar-cap averaged zonal wind decreases significantly when increasing the number of stations and array data parameters. In contrast, for the year 2020, with no major SSW and less stratospheric vortex variability, the RMSE is persistent across the different number of stations and array data parameters included in the training.

In addition to the nowcasting methodology applied in this work, a forecasting training methodology is available through the Delay-SDE-net framework (Eggen & Midtjord, 2023), and these capabilities might be utilized to forecast the stratospheric circulation in future studies. Further numerical experiments can also be conducted to assess to what extent stratospheric wind forecasting benefits from being informed with infrasound data in addition to the present and past stratospheric wind and temperature.

This study confirms that microbarom observations carry valuable information about the upper stratospheric dynamics, thus highlighting the potential to use near-real-time IMS infrasound data in stratospheric diagnostics. The only previously published infrasound data assimilation studies are offline experiments that provide a more localized stratospheric probing using signals from explosive events (Amezcuca *et al.*, 2020; Amezcuca & Barton, 2021). A long-term goal is to develop data assimilation approaches for microbarom infrasound, contributing to an enhanced upper stratospheric dynamics representation in atmospheric models, and ultimately to improve the subseasonal-to-seasonal forecast skill.

AUTHOR CONTRIBUTIONS

Ekaterina Vorobeva: methodology; data curation; formal analysis; investigation; software; validation;

visualization; writing-original draft; writing-review & editing. **Mari Dahl Eggen**: methodology; data curation; formal analysis; investigation; software; validation; visualization; writing-original draft; writing-review & editing. **Alise Danielle Midtjord**: software; validation; writing-review&editing. **Fred Espen Benth**: project administration; supervision; writing-review & editing. **Patrick Hupe**: data curation; software; investigation; writing-review & editing. **Quentin Brissaud**: investigation; validation; writing-review & editing. **Yvan Orsolini**: investigation; validation; writing-review & editing. **Sven Peter Näsholm**: conceptualization; funding acquisition; investigation; methodology; project administration; supervision; validation; writing-original draft; writing-review and editing.

ACKNOWLEDGMENTS

We thank Sarah Albert and an anonymous reviewer for useful comments that improved our article. Special thanks to Patrick Espy for helpful discussions and for facilitating the incorporation of the study into the Birkeland Center for Space Science (BCSS) project. We thank Jelle Assink, Láslo Evers, Tormod Kværna, Alexis Le Pichon, and Constantino Listowski for fruitful discussions. This research was supported by the Research Council of Norway FRIPRO/FRINATEK basic research program, project contract 274377: *Middle Atmosphere Dynamics: Exploiting Infrasound Using a Multidisciplinary Approach at High Latitudes* (MADEIRA). It was also supported by the BCSS project under Research Council of Norway contract 223252/F50. The PhD grant of Mari Dahl Eggen is funded by NORSAR. This study was facilitated by previous research carried out within the framework of the ARISE and ARISE2 projects (Blanc *et al.*, 2018, 2019).

CONFLICT OF INTEREST STATEMENT

The authors declare no conflicts of interest.

DATA AVAILABILITY STATEMENT

Hourly ERA5 wind fields on pressure levels are available for download at the Climate Data Store website, <https://cds.climate.copernicus.eu/cdsapp#!/dataset/>. Global microbarom observations at the IMS infrasound network processed using PMCC are openly available via the Geoportal of the German Federal Institute for Geosciences and Natural Resources (BGR) at <https://doi.org/10.25928/bgrseis&uscore;mbfl-ifs.d>. The Delay-SDE-net model code is available at <https://github.com/alimid/Delay-SDE-net>.

ORCID

Ekaterina Vorobeva  <https://orcid.org/0000-0001-7680-5014>

Mari Dahl Eggen  <https://orcid.org/0000-0001-6952-672X>

Alise Danielle Midtjord  <https://orcid.org/0000-0001-5906-7988>

Fred Espen Benth  <https://orcid.org/0000-0001-9907-6811>

Patrick Hupe  <https://orcid.org/0000-0003-0864-812X>

Quentin Brissaud  <https://orcid.org/0000-0001-8189-4699>

Yvan Orsolini  <https://orcid.org/0000-0001-7454-026X>

Sven Peter Näsholm  <https://orcid.org/0000-0001-9107-4002>

REFERENCES

- Albert, S. & Linville, L. (2020) Benchmarking current and emerging approaches to infrasound signal classification. *Seismological Research Letters*, 91, 921–929. Available from: <https://doi.org/10.1785/0220190116>
- Albert, S.A. (2022) Atmospheric structure prediction for infrasound propagation modeling using deep learning. *Earth and Space Science*, 9, e2022EA002233. Available from: <https://doi.org/10.1029/2022EA002233>
- Amezcuca, J. & Barton, Z. (2021) Assimilating atmospheric infrasound data to constrain atmospheric winds in a two-dimensional grid. *Quarterly Journal of the Royal Meteorological Society*, 147, 3530–3554. Available from: <https://doi.org/10.1002/qj.4141>
- Amezcuca, J., Näsholm, S.P., Blixt, E.M. & Charlton-Perz, A.J. (2020) Assimilation of atmospheric infrasound data to constrain tropospheric and stratospheric winds. *Quarterly Journal of the Royal Meteorological Society*, 146, 2634–2653. Available from: <https://doi.org/10.1002/qj.3809>
- Baldwin, M.P., Ayarzagüena, B., Birner, T., Butchart, N., Butler, A.H., Charlton-Perez, A.J. et al. (2021) Sudden stratospheric warmings. *Reviews of Geophysics*, 59, e2020RG000708. Available from: <https://doi.org/10.1029/2020RG000708>
- Baldwin, M.P. & Dunkerton, T.J. (2001) Stratospheric harbingers of anomalous weather regimes. *Science*, 294, 581–584. Available from: <https://doi.org/10.1126/science.1063315>
- Basse-O'Connor, A., Slot Nielsen, M., Pedersen, J. & Rohde, V. (2020) Stochastic delay differential equations and related autoregressive models. *Stochastics*, 92, 454–477. Available from: <https://doi.org/10.1080/17442508.2019.1635601>
- Bell, B., Hersbach, H., Simmons, A., Berrisford, P., Dahlgren, P., Horányi, A. et al. (2021) The ERA5 global reanalysis: preliminary extension to 1950. *Quarterly Journal of the Royal Meteorological Society*, 147, 4186–4227. Available from: <https://doi.org/10.1002/qj.4174>
- Ben-Bouallegue, Z., Clare, M.C., Magnusson, L., Gascon, E., Maier-Gerber, M., Janousek, M. et al. (2023) The rise of data-driven weather forecasting. *Arxiv*. [Preprint] Available from: <https://doi.org/10.48550/arXiv.2307.10128>
- Benioff, H. & Gutenberg, B. (1939) Waves and currents recorded by electromagnetic barographs. *Bulletin of the American Meteorological Society*, 20, 421–428. Available from: <https://doi.org/10.1175/1520-0477-20.10.421>
- Benth, F.E., Šaltytė Benth, J. & Koekebakker, S. (2008) *Stochastic modelling of electricity and related markets*. *Advanced series on*

- statistical science & applied probability*, Vol. 11. Singapore: World Scientific Publishing Co. Pte. Ltd. Available from: <https://doi.org/10.1142/6811>
- Benth, J.S. & Benth, F.E. (2010) Analysis and modelling of wind speed in New York. *Journal of Applied Statistics*, 37, 893–909. Available from: <https://doi.org/10.1080/02664760902914490>
- Bishop, J.W., Blom, P.S., Webster, J., Reichard-Flynn, W. & Lin, Y. (2022) Deep learning categorization of infrasound array data. *The Journal of the Acoustical Society of America*, 152, 2434–2445. Available from: <https://doi.org/10.1121/10.0014903>
- Blanc, E., Ceranna, L., Hauchecorne, A., Charlton-Perez, A., Marchetti, E., Evers, L. et al. (2018) Toward an improved representation of middle atmospheric dynamics thanks to the ARISE project. *Surveys in Geophysics*, 39, 171–225. Available from: <https://doi.org/10.1007/s10712-017-9444-0>
- Blanc, E., Pol, K., Le Pichon, A., Hauchecorne, A., Keckhut, P., Baumgarten, G. et al. (2019) Middle atmosphere variability and model uncertainties as investigated in the framework of the ARISE project. In: Le Pichon, A., Blanc, E. & Hauchecorne, A. (Eds.) *Infrasound monitoring for atmospheric studies*. Cham: Springer, pp. 845–887. Available from: https://doi.org/10.1007/978-3-319-75140-5_28
- Brissaud, Q. & Astafyeva, E. (2022) Near-real-time detection of co-seismic ionospheric disturbances using machine learning. *Geophysical Journal International*, 230, 2117–2130. Available from: <https://doi.org/10.1093/gji/ggac167>
- Brissaud, Q., Näsholm, S.P., Turquet, A. & Le Pichon, A. (2023) Predicting infrasound transmission loss using deep learning. *Geophysical Journal International*, 232, 274–286. Available from: <https://doi.org/10.1093/gji/ggac307>
- Brockwell, P.J. (2004) Representations of continuous-time ARMA processes. *Journal of Applied Probability*, 41, 375–382. Available from: <https://doi.org/10.1239/jap/1082552212>
- Brockwell, P.J. (2014) Recent results in the theory and applications of CARMA processes. *Annals of the Institute of Statistical Mathematics*, 66, 647–685. Available from: <https://doi.org/10.1007/s10463-014-0468-7>
- Brockwell, P.J. & Davis, R.A. (2016) *Introduction to time series and forecasting*. Cham: Springer. Available from: <https://doi.org/10.1007/978-3-319-29854-2>
- Broszkiewicz-Suwaj, E. & Wylomańska, A. (2021) Application of non-Gaussian multidimensional autoregressive model for climate data prediction. *International Journal of Advances in Engineering Sciences and Applied Mathematics*, 13, 236–247. Available from: <https://doi.org/10.1007/s12572-021-00300-1>
- Butler, A.H., Seidel, D.J., Hardiman, S.C., Butchart, N., Birner, T. & Match, A. (2015) Defining sudden stratospheric warmings. *Bulletin of the American Meteorological Society*, 96, 1913–1928. Available from: <https://doi.org/10.1175/BAMS-D-13-00173.1>
- Butler, A.H., Sjöberg, J.P., Seidel, D.J. & Rosenlof, K.H. (2017) A sudden stratospheric warming compendium. *Earth System Science Data*, 9, 63–76. Available from: <https://doi.org/10.5194/essd-9-63-2017>
- Campbell, S.D. & Diebold, F.X. (2005) Weather forecasting for weather derivatives. *Journal of the American Statistical Association*, 100, 6–16. Available from: <https://doi.org/10.1198/016214504000001051>
- Cansi, Y. (1995) An automatic seismic event processing for detection and location: the P.M.C.C. method. *Geophysical Research Letters*, 22, 1021–1024. Available from: <https://doi.org/10.1029/95GL00468>
- Cansi, Y. & Le Pichon, A. (2008) Infrasound event detection using the progressive multi-channel correlation algorithm. In: Havelock, D., Kuwano, S. & Vorländer, M. (Eds.) *Handbook of signal processing in acoustics*. New York: Springer, pp. 1425–1435. Available from: https://doi.org/10.1007/978-0-387-30441-0_77
- Charlton-Perez, A.J., Dacre, H.F., Driscoll, S., Gray, S.L., Harvey, B., Harvey, N.J. et al. (2023) Do AI models produce better weather forecasts than physics-based models? A quantitative evaluation case study of Storm Ciarán. *Arxiv*. [Preprint] Available from: <http://arxiv.org/abs/2312.02658>
- Chen, R.T., Rubanova, Y., Bettencourt, J. & Duvenaud, D.K. (2018) Neural ordinary differential equations. *Advances in Neural Information Processing Systems*, 31.
- Cheng, S., Quilodrán-Casas, C., Ouala, S., Farchi, A., Liu, C., Tandeo, P. et al. (2023) Machine learning with data assimilation and uncertainty quantification for dynamical systems: a review. *IEEE/CAA Journal of Automatica Sinica*, 10, 1361–1387. Available from: <https://doi.org/10.1109/JAS.2023.123537>
- Cohen, J., Coumou, D., Hwang, J., Mackey, L., Orenstein, P., Totz, S. et al. (2019) S2S reboot: an argument for greater inclusion of machine learning in subseasonal to seasonal forecasts. *Wiley Interdisciplinary Reviews: Climate Change*, 10, e00567. Available from: <https://doi.org/10.1002/wcc.567>
- De Carlo, M., Ardhuin, F. & Le Pichon, A. (2020) Atmospheric infrasound generation by ocean waves in finite depth: unified theory and application to radiation patterns. *Geophysical Journal International*, 221, 569–585. Available from: <https://doi.org/10.1093/gji/ggaa015>
- De Carlo, M., Hupe, P., Le Pichon, A., Ceranna, L. & Ardhuin, F. (2021) Global microbarom patterns: a first confirmation of the theory for source and propagation. *Geophysical Research Letters*, 48, e2020GL090163. Available from: <https://doi.org/10.1029/2020GL090163>
- Dee, D.P., Uppala, S.M., Simmons, A.J., Berrisford, P., Poli, P., Kobayashi, S. et al. (2011) The ERA-interim reanalysis: configuration and performance of the data assimilation system. *Quarterly Journal of the Royal Meteorological Society*, 137, 553–597.
- Der Kiureghian, A. & Ditlevsen, O. (2009) Aleatory or epistemic? Does it matter? *Structural Safety*, 31, 105–112.
- Devore, J.L., Berk, K.N. & Carlton, M.A. (2012) *Modern mathematical statistics with applications*, Vol. 285. Cham: Springer.
- Diamond, M. (1963) Sound channels in the atmosphere. *Journal of Geophysical Research*, 68, 3459–3464. Available from: <https://doi.org/10.1029/JZ068i011p03459>
- Domeisen, D.I., Butler, A.H., Charlton-Perez, A.J., Ayarzagüena, B., Baldwin, M.P., Dunn-Sigouin, E. et al. (2020a) The role of the stratosphere in subseasonal to seasonal prediction: 1. Predictability of the stratosphere. *Journal of Geophysical Research: Atmospheres*, 125, e2019JD030920. Available from: <https://doi.org/10.1029/2019JD030920>
- Domeisen, D.I.V., Butler, A.H., Charlton-Perez, A.J., Ayarzagüena, B., Baldwin, M.P., Dunn-Sigouin, E. et al. (2020b) The role of the stratosphere in subseasonal to seasonal prediction: 2. Predictability arising from stratosphere-troposphere coupling. *Journal of Geophysical Research: Atmospheres*, 125, e2019JD030923. Available from: <https://doi.org/10.1029/2019JD030923>

- Donn, W.L. & Rind, D. (1971) Natural infrasound as an atmospheric probe. *Geophysical Journal International*, 26, 111–133. Available from: <https://doi.org/10.1111/j.1365-246X.1971.tb03386.x>
- Drob, D.P., Picone, J. & Garcés, M. (2003) Global morphology of infrasound propagation. *Journal of Geophysical Research: Atmospheres*, 4608, 1–12. Available from: <https://doi.org/10.1029/2002JD003307>
- Eggen, M.D. (2022) The multivariate ARMA/CARMA transformation relation. *Arxiv*. [Preprint] Available from: <https://arxiv.org/abs/2205.05080>
- Eggen, M.D., Dahl, K.R., Näsholm, S.P. & Mæland, S. (2022) Stochastic modeling of stratospheric temperature. *Mathematical Geosciences*, 54, 651–678. Available from: <https://doi.org/10.1007/s11004-021-09990-6>
- Eggen, M.D. & Midtjord, A.D. (2023) Delay-SDE-net: a deep learning approach for time series modelling with memory and uncertainty estimates. *Arxiv*. [Preprint] Available from: <https://doi.org/10.48550/arXiv.2303.08587>
- Eswaraiah, S., Kumar, K.N., Kim, Y.H., Chalapathi, G.V., Lee, W., Jiang, G. et al. (2020) Low-latitude mesospheric signatures observed during the 2017 sudden stratospheric warming using the Fuke meteor radar and ERA-5. *Journal of Atmospheric and Solar-Terrestrial Physics*, 207, 105352. Available from: <https://doi.org/10.1016/j.jastp.2020.105352>
- Eswaraiah, S., Venkat Ratnam, M., Kim, Y.H., Kumar, K.N., Venkata Chalapathi, G., Ramanajaneyulu, L. et al. (2019) Advanced meteor radar observations of mesospheric dynamics during 2017 minor SSW over the tropical region. *Advances in Space Research*, 64, 1940–1947. Available from: <https://doi.org/10.1016/j.asr.2019.05.039>
- Garcés, M., Willis, M., Hetzer, C., Le Pichon, A. & Drob, D. (2004) On using ocean swells for continuous infrasonic measurements of winds and temperature in the lower, middle, and upper atmosphere. *Geophysical Research Letters*, 31, L19304. Available from: <https://doi.org/10.1029/2004GL020696>
- Gómez, V. (2019) *Linear time series with MATLAB and OCTAVE*. Cham: Springer International Publishing. Imprint: Springer. Available from: <https://doi.org/10.1007/978-3-030-20790-8>
- Hayashi, K. & Nakagawa, K. (2022) Fractional SDE-net: generation of time series data with long-term memory. In: *2022 IEEE 9th international conference on data science and advanced analytics (DSAA)*. New York: IEEE, pp. 1–10. Available from: <https://doi.org/10.1109/DSAA54385.2022.10032351>
- Hersbach, H., Bell, B., Berrisford, P., Hirahara, S., Horányi, A., Muñoz-Sabater, J. et al. (2020) The ERA5 global reanalysis. *Quarterly Journal of the Royal Meteorological Society*, 146, 1999–2049. Available from: <https://doi.org/10.1002/qj.3803>
- Högbom, J.A. (1974) Aperture synthesis with a non-regular distribution of interferometer baselines. *Astronomy and Astrophysics Supplement Series*, 15, 417.
- Hupe, P., Ceranna, L., Le Pichon, A., Matoza, R.S. & Mialle, P. (2021) Microbarom low-frequency data products of the international monitoring system's infrasound stations [data set]. Available at: https://doi.org/10.25928/bgrseis_mblf-ifs
- Hupe, P., Ceranna, L., Le Pichon, A., Matoza, R.S. & Mialle, P. (2022) International monitoring system infrasound data products for atmospheric studies and civilian applications. *Earth System Science Data*, 14, 4201–4230. Available from: <https://doi.org/10.5194/essd-14-4201-2022>
- Hupe, P., Ceranna, L., Pilger, C., De Carlo, M., Le Pichon, A., Kailer, B. et al. (2019) Assessing middle atmosphere weather models using infrasound detections from microbaroms. *Geophysical Journal International*, 216, 1761–1767. Available from: <https://doi.org/10.1093/gji/ggy520>
- de Jesus, R., Batista, I.S., Jonah, O.F., de Abreu, A.J., Fagundes, P.R., Venkatesh, K. et al. (2017) An investigation of the ionospheric disturbances due to the 2014 sudden stratospheric warming events over Brazilian sector. *Journal of Geophysical Research: Space Physics*, 122, 11698–11715. Available from: <https://doi.org/10.1002/2017JA024560>
- Johnson, S.J., Stockdale, T.N., Ferranti, L., Balmaseda, M.A., Molteni, F., Magnusson, L. et al. (2019) SEAS5: the new ECMWF seasonal forecast system. *Geoscientific Model Development*, 12, 1087–1117. Available from: <https://doi.org/10.5194/gmd-12-1087-2019>
- Karpechko, A.Y. (2018) Predictability of sudden stratospheric warmings in the ECMWF extended-range forecast system. *Monthly Weather Review*, 146, 1063–1075. Available from: <https://doi.org/10.1175/MWR-D-17-0317.1>
- Kolstad, E.W., Breiteig, T. & Scaife, A.A. (2010) The association between stratospheric weak polar vortex events and cold air outbreaks in the northern hemisphere. *Quarterly Journal of the Royal Meteorological Society*, 136, 886–893. Available from: <https://doi.org/10.1002/qj.620>
- Kong, L., Sun, J. & Zhang, C. (2020) SDE-Net: Equipping deep neural networks with uncertainty estimates. *Arxiv*. [Preprint] Available from: <http://arxiv.org/abs/2008.10546>
- Kristoffersen, S.K., Le Pichon, A., Hupe, P. & Matoza, R.S. (2022) Updated global reference models of broadband coherent infrasound signals for atmospheric studies and civilian applications. *Earth and Space Science*, 9, e2022EA002222. Available from: <https://doi.org/10.1029/2022EA002222>
- Lam, R., Sanchez-Gonzalez, A., Willson, M., Wirnsberger, P., Fortunato, M., Alet, F. et al. (2023) Learning skillful medium-range global weather forecasting. *Science*, 382, 1416–1421. Available from: <https://doi.org/10.1126/science.adi2336>
- Landès, M., Ceranna, L., Le Pichon, A. & Matoza, R.S. (2012) Localization of microbarom sources using the IMS infrasound network. *Journal of Geophysical Research: Atmospheres*, 117, D06102. Available from: <https://doi.org/10.1029/2011JD016684>
- Le Pichon, A., Blanc, E. & Hauchecorne, A. (2010) *Infrasound monitoring for atmospheric studies*. Cham: Springer. Available from: <https://doi.org/10.1007/978-1-4020-9508-5>
- Le Pichon, A., Blanc, E. & Hauchecorne, A. (2019) *Infrasound monitoring for atmospheric studies: challenges in middle atmosphere dynamics and societal benefits*. Cham: Springer.
- Le Pichon, A., Ceranna, L., Garcés, M., Drob, D. & Millet, C. (2006) On using infrasound from interacting ocean swells for global continuous measurements of winds and temperature in the stratosphere. *Journal of Geophysical Research: Atmospheres*, 111, 1–7. Available from: <https://doi.org/10.1029/2005JD006690>
- Limpasuvan, V., Hartmann, D.L., Thompson, D.W., Jeev, K. & Yung, Y.L. (2005) Stratosphere-troposphere evolution during polar vortex intensification. *Journal of Geophysical Research: Atmospheres*, 110, D24101. Available from: <https://doi.org/10.1029/2005JD006302>
- Limpasuvan, V., Orsolini, Y.J., Chandran, A., Garcia, R.R. & Smith, A.K. (2016) On the composite response of the MLT to major sudden stratospheric warming events with elevated stratopause.

- Journal of Geophysical Research: Atmospheres*, 121, 4518–4537. Available from: <https://doi.org/10.1002/2015jd024401>
- Liszka, L. (2008) *Listening to meteors: infrasonic observations of meteors in northern Sweden*. Swedish Institute of Space Physics.
- Manney, G.L. & Lawrence, Z.D. (2016) The major stratospheric final warming in 2016: dispersal of vortex air and termination of Arctic chemical ozone loss. *Atmospheric Chemistry & Physics*, 16, 15371–15396. Available from: <https://doi.org/10.5194/acp-16-15371-2016>
- Manney, G.L., Lawrence, Z.D., Santee, M.L., Read, W.G., Livesey, N.J., Lambert, A. et al. (2015) A minor sudden stratospheric warming with a major impact: transport and polar processing in the 2014/2015 Arctic winter. *Geophysical Research Letters*, 42, 7808–7816. Available from: <https://doi.org/10.5194/acp-16-15371-2016>
- Marquardt, T. & Stelzer, R. (2007) Multivariate CARMA processes. *Stochastic Processes and their Applications*, 117, 96–120. Available from: <https://doi.org/10.1016/j.spa.2006.05.014>
- Marty, J. (2019) The IMS infrasound network: current status and technological developments. In: Le Pichon, A., Blanc, E. & Hauchecorne, A. (Eds.) *Infrasound monitoring for atmospheric studies: challenges in middle atmosphere dynamics and societal benefits*. Cham: Springer, pp. 3–62. Available from: https://doi.org/10.1007/978-3-319-75140-5_1
- Øksendal, B. (2003) *Stochastic differential equations: an introduction with applications*, 6th edition. Berlin: Springer. Available from: <https://doi.org/10.1007/978-3-642-14394-6>.
- Orsolini, Y.J., Nishii, K. & Nakamura, H. (2018) Duration and decay of Arctic stratospheric vortex events in the ECMWF seasonal forecast model. *Quarterly Journal of the Royal Meteorological Society*, 144, 2876–2888. Available from: <https://doi.org/10.1002/qj.3417>
- Orsolini, Y.J., Zhang, J. & Limpasuvan, V. (2022) Abrupt change in the lower thermospheric mean meridional circulation during sudden stratospheric warmings and its impact on trace species. *Journal of Geophysical Research: Atmospheres*, 127, e2022JD037050. Available from: <https://doi.org/10.1029/2022JD037050>
- den Ouden, O.F.C., Assink, J.D., Smets, P.S.M., Shani-Kadmiel, S., Averbuch, G. & Evers, L.G. (2020) CLEAN beamforming for the enhanced detection of multiple infrasonic sources. *Geophysical Journal International*, 221, 305–317. Available from: <https://doi.org/10.1093/gji/ggaa010>
- Pedatella, N., Chau, J., Schmidt, H., Goncharenko, L., Stolle, C., Hocke, K. et al. (2018) How sudden stratospheric warmings affect the whole atmosphere. *Eos*, 35–38. Available from: <https://doi.org/10.1029/2018EO092441>
- Pedatella, N.M. (2023) Influence of stratosphere polar vortex variability on the mesosphere, thermosphere, and ionosphere. *Journal of Geophysical Research: Space Physics*, 128, e2023JA031495. Available from: <https://doi.org/10.1029/2023JA031495>
- Pérot, K. & Orsolini, Y.J. (2021) Impact of the major SSWs of February 2018 and January 2019 on the middle atmospheric nitric oxide abundance. *Journal of Atmospheric and Solar-Terrestrial Physics*, 218, 105586. Available from: <https://doi.org/10.1016/j.jastp.2021.105586>
- Raissi, M., Perdikaris, P. & Karniadakis, G.E. (2019) Physics-informed neural networks: a deep learning framework for solving forward and inverse problems involving nonlinear partial differential equations. *Journal of Computational Physics*, 378, 686–707. Available from: <https://doi.org/10.1016/j.jcp.2018.10.045>
- Rao, J., Garfinkel, C.I., Chen, H. & White, I.P. (2019) The 2019 new year stratospheric sudden warming and its real-time predictions in multiple S2S models. *Journal of Geophysical Research: Atmospheres*, 124, 11155–11174. Available from: <https://doi.org/10.1029/2019JD030826>
- Rao, J., Ren, R., Chen, H., Yu, Y. & Zhou, Y. (2018) The stratospheric sudden warming event in February 2018 and its prediction by a climate system model. *Journal of Geophysical Research: Atmospheres*, 123, 13–332. Available from: <https://doi.org/10.1029/2018JD028908>
- Rind, D. & Donn, W.L. (1975) Further use of natural infrasound as a continuous monitor of the upper atmosphere. *Journal of the Atmospheric Sciences*, 32, 1694–1704. Available from: [https://doi.org/10.1175/1520-0469\(1975\)032<#x0003C;1694:FUONIA>2.0.CO;2](https://doi.org/10.1175/1520-0469(1975)032<#x0003C;1694:FUONIA>2.0.CO;2)
- Scaife, A., Karpechko, A.Y., Baldwin, M., Brookshaw, A., Butler, A., Eade, R. et al. (2016) Seasonal winter forecasts and the stratosphere. *Atmospheric Science Letters*, 17, 51–56. Available from: <https://doi.org/10.1002/asl.598>
- Scaife, A.A., Baldwin, M.P., Butler, A.H., Charlton-Perez, A.J., Domeisen, D.I.V., Garfinkel, C.I. et al. (2022) Long-range prediction and the stratosphere. *Atmospheric Chemistry and Physics*, 22, 2601–2623. Available from: <https://doi.org/10.5194/acp-22-2601-2022>
- Schultz, M.G., Betancourt, C., Gong, B., Kleinert, F., Langguth, M., Leufen, L.H. et al. (2021) Can deep learning beat numerical weather prediction? *Philosophical Transactions of the Royal Society A*, 379, 20200097. Available from: <https://doi.org/10.1098/rsta.2020.0097>
- Shepherd, M.G., Beagley, S.R. & Fomichev, V.I. (2014) Stratospheric warming influence on the mesosphere/lower thermosphere as seen by the extended CMAM. *Annales Geophysicae*, 32, 589–608. Available from: <https://angeo.copernicus.org/articles/32/589/2014/>
- Vignon, E. & Mitchell, D.M. (2015) The stratopause evolution during different types of sudden stratospheric warming event. *Climate Dynamics*, 44, 3323–3337. Available from: <https://doi.org/10.1007/s00382-014-2292-4>
- Vorobeva, E., De Carlo, M., Le Pichon, A., Espy, P.J. & Näsholm, S.P. (2021) Benchmarking microbarom radiation and propagation model against infrasound recordings: a vespagram-based approach. *Annales Geophysicae*, 39, 515–531. Available from: <https://doi.org/10.5194/angeo-39-515-2021>
- Wang, Y., Tan, H. & Yao, S. (2021) Curved SDE-net leads to better generalization for uncertainty estimates of DNNs. In: Farkaš, I., Masulli, P., Otte, S. & Wermter, S. (Eds.) *Artificial neural networks and machine learning—ICANN 2021*. Cham: Springer International Publishing, pp. 248–259. Available from: https://doi.org/10.1007/978-3-030-86340-1_20
- Waugh, D.W., Sobel, A.H. & Polvani, L.M. (2017) What is the polar vortex and how does it influence weather? *Bulletin of the American Meteorological Society*, 98, 37–44. Available from: <https://doi.org/10.1175/BAMS-D-15-00212.1>
- Witsil, A., Fee, D., Dickey, J., Peña, R., Waxler, R. & Blom, P. (2022) Detecting large explosions with machine learning models trained on synthetic infrasound data. *Geophysical Research*

- Letters*, 49, e2022GL097785. Available from: <https://doi.org/10.1029/2022GL097785>
- Yin, S., Ma, Z., Gong, Y., Zhang, S. & Li, G. (2023) Response of quasi-10-day waves in the MLT region to the sudden stratospheric warming in march 2020. *Advances in Space Research*, 71, 298–305. Available from: <https://doi.org/10.1016/j.asr.2022.10.054>
- Zülicke, C. & Becker, E. (2013) The structure of the mesosphere during sudden stratospheric warmings in a global circulation model. *Journal of Geophysical Research: Atmospheres*, 118, 2255–2271. Available from: <https://doi.org/10.1002/jgrd.50219>

How to cite this article: Vorobeva, E., Eggen, M.D., Midtjord, A.D., Benth, F.E., Hupe, P., Brissaud, Q. *et al.* (2024) Estimating stratospheric polar vortex strength using ambient ocean-generated infrasound and stochastics-based machine learning. *Quarterly Journal of the Royal Meteorological Society*, 1–15. Available from: <https://doi.org/10.1002/qj.4731>